Optics Communications 592 (2025) 132137

Contents lists available at ScienceDirect

Optics Communications

journal homepage: www.elsevier.com/locate/optcom

# An expanded theory on moving Fabry–Perot interferometers and its application to Pound-Drever-Hall frequency locking

Lingze Duan

*Department of Physics and Astronomy, The University of Alabama in Huntsville, Huntsville, AL, 35899, USA*

ARTICLE INFO

*Keywords:*
Fabry–Perot interferometers
Optical interferometry
Doppler effect
Pound-Drever-Hall technique
Transmission coefficient
Reflection coefficient
Laser frequency locking

ABSTRACT

In this paper, we analyze the impact of velocity on the optical response of a passive Fabry–Perot interferometer (FPI), seeking to establish an analytical framework that describes the transmission and reflection properties of the FPI when key components in its operation system, including the light source, the detector and the interferometer itself, have relative motions relative to each other along their common optical axis. Our analysis indicates that these movements result in additional Doppler-induced factors in the transmission and reflection coefficients, and these factors lead to new effects that are sensitive to velocity. To demonstrate its potential application, the theory is applied to the Pound-Drever-Hall frequency-locking technique. It is shown that velocity-induced frequency modulations are effectively added to the laser frequency due to the motions, and such excess frequency noise can be impactful in certain applications.

## 1. Introduction

The Fabry–Perot interferometer (FPI) is a versatile optical device widely used in precision measurement, sensing, and spectroscopy [1]. It is capable of achieving very high wavelength resolutions through the phenomenon of multiple beam interference between two parallel reflective surfaces. Since its invention more than a century ago [2], considerable effort has been devoted to expanding the applications of the FPI. Much less attention, however, has been paid to scrutinizing its basic operating principle, especially when motion is involved.

The impact of motion on the optical properties of the FPI has become a relevant question in recent years, largely due to the emergence of hybrid interferometers, where an FPI is often nested in a host interferometer to serve as a multiplier of the optical path [3–6]. Because the host interferometer is very sensitive to the transmission phase of the FPI, any phase shift induced by the motion of the FPI would contribute to the output of the hybrid interferometer. To accurately analyze such scenarios, a generalization of the conventional theory of FPI to include the effects of motion becomes necessary.

Meanwhile, optical clocks and high-precision frequency references often rely on passive FPIs to regulate optical frequencies [7]. However, mechanical instabilities often become a limiting factor in their performance [8,9]. The impacts of such instabilities have been extensively studied by examining induced displacements [8,10]. But never before has velocity been considered as a potential source of excess noise. A thorough investigation of that aspect would also require a generalized FPI theory with the effects of motion incorporated in it.

Previously, we discussed the difference between a moving FPI and a conventional scanning FPI. A moving FPI refers to an FPI moving as a rigid body with its length (i.e., the spacing between its two mirrors) remaining constant, whereas in a scanning FPI, the spacing between the two mirrors is tuned so that the length of the FPI changes, as illustrated in Fig. 1. While it is well known that scanning the mirror spacing leads to a change of the free spectral range (FSR), it is less obvious what optical property changes when the FPI moves as a whole. In our prior report [11], we studied the transmission properties of a moving FPI and pointed out that a uniform motion of the FPI along its optical axis results in a velocity-dependent rescaling of the round trip phase in the transmission coefficient.

However, an important aspect that was not addressed in our previous work is the fundamental cause of this phase rescaling. It is tempting to simply attribute this new velocity-dependent factor to the Doppler shift caused by the relative motion between the FPI and the incident light source. This perception turns out to be inaccurate as it fails to account for the impact of the observer in the overall FPI operation scheme, as will be shown later in this paper. It hence becomes clear that a thorough understanding of the optical properties of a moving FPI requires a theory that takes into account not only the FPI itself, but also its interrogation system. Moreover, many practical applications of the FPI use it in reflection rather than in transmission. This necessitates a close look at the reflection coefficient of a moving FPI in addition to its transmission coefficient.

*E-mail address:* lingze.duan@uah.edu.

https://doi.org/10.1016/j.optcom.2025.132137
Received 24 March 2025; Received in revised form 14 June 2025; Accepted 16 June 2025
Available online 16 July 2025

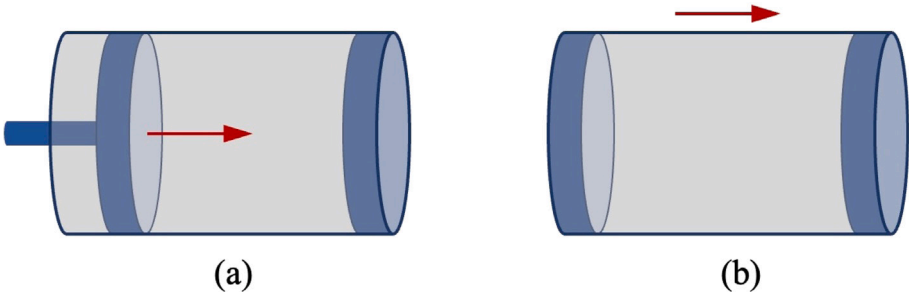


**Fig. 1.** The conceptual difference between (a) a scanning FPI, where a moving mirror changes the effective length of the FPI, and (b) a moving FPI, where the entire FPI moves as a rigid body with its length remaining constant.

The current paper seeks to address this inadequacy by expanding the discussion of a moving FPI to include the states of motion of the light source and the detector, effectively treating the FPI as part of a "three-body"system rather than as an isolated device. We will also investigate the reflection of the FPI in addition to the transmission. As such, we are able to establish an expanded theory for the FPI when motion is involved in its operation. In the second half of the paper, we will showcase the application of the new theory by evaluating the impacts of motions on laser frequency locking based on the Pound-Drever-Hall (PDH) technique.

## 2. General theory of moving FPI

Let us first define the system under study. In this work, we focus on passive FPIs, whose operation involves three key components: a light source, an FPI, and a detector, as shown conceptually in Fig. 2(a). In principle, all three components can move independently along their common optical axis. Since the action of "observation" is carried out effectively by the detector in the current context, without losing any generality, we consider the detector as the "observer" and define its frame as the "lab frame". The states of motion of the other two components in the lab frame create four scenarios, depicted here in Fig. 2(a)–(d): (a) both the light source and the FPI are stationary; (b) the light source is stationary while the FPI is moving; (c) the light source is moving while the FPI is stationary; (d) both the light source and the FPI are moving. Note that these are four distinct scenarios, which cannot be duplicated by one another as will be discussed in the following.

Here are some general conditions we follow throughout this paper. The FPI is treated as a rigid body without deformation. All motions are considered uniform, that is, at constant velocities. This generally suffices because, as previously shown [11], nonuniform motions can be fairly well described by a simple generalization of the uniform motion model within a wide range of accelerations. Finally, all discussions are confined to the nonrelativistic regime given the negligible impact of relativistic effects for most applications [11].

### 2.1. Stationary light source and stationary FPI

We begin with the simplest case, where both the light source and the FPI are fixed in the lab frame and hence remain stationary to the detector (i.e., the observer) as shown in Fig. 2(a). This is the conventional way of operating the FPI. We can directly write out the transmission and the reflection coefficients of the FPI as

$$T \equiv \frac{\mathcal{E}_T}{\mathcal{E}_I} = \frac{(1-r^2)e^{-inkd}}{1-r^2e^{-2inkd}}, \tag{1}$$

and

$$R \equiv \frac{\mathcal{E}_R}{\mathcal{E}_I} = \frac{r(1-e^{-2inkd})}{1-r^2e^{-2inkd}}, \tag{2}$$

where $\mathcal{E}_I$, $\mathcal{E}_R$ and $\mathcal{E}_T$ are the electric fields of the incident, reflected and transmitted waves, respectively, and $k$ is the wave number in vacuum. The reflection coefficients of the two mirrors are assumed to be identical here and are denoted as $r$. With a proper length $d$, the FPI is considered to be made of a homogeneous, isotropic, and lossless optical medium of refractive index $n$. The corresponding FPI transmittance and reflectance are given by

$$|T|^2 = \frac{1}{1+(2\mathcal{F}/\pi)^2\sin^2(nkd)}, \tag{3}$$

and

$$|R|^2 = \frac{(2\mathcal{F}/\pi)^2\sin^2(nkd)}{1+(2\mathcal{F}/\pi)^2\sin^2(nkd)}, \tag{4}$$

where $\mathcal{F} = \pi r/(1-r^2)$ is the finesse of the FPI.

### 2.2. Stationary light source and moving FPI

Let us move on to the second case, where the light source is fixed in the lab frame while the FPI is traveling uniformly along the optical axis, as shown in Fig. 2(b). We have previously analyzed this case for optical transmission and have shown that a velocity-dependent scaling factor needs to be added to the round-trip phase to account for the effect of the uniform motion [11]. The resulting transmission coefficient can be written as

$$T = \frac{(1-r^2)e^{-i\zeta nkd}}{1-r^2e^{-2i\zeta nkd}}, \tag{5}$$

where $\zeta$ is defined as

$$\zeta = \sqrt{\frac{c-v_i}{c+v_i}}, \tag{6}$$

with $v_i$ and $c$ being the velocity of the interferometer and the speed of light in vacuum, respectively.

To find the FPI reflection coefficient, we follow the same strategy as previously used to derive the transmission coefficient and construct the superposition of consecutively reflected wavefronts [11]. Fig. 3 conceptually illustrates this process. First, we note that, unlike transmission, waves reflected off a uniformly moving FPI have a different frequency from the incident wave due to the Doppler effect. At any moment of time, if the incident field on the input plane of the FPI is denoted as $\mathcal{E}_I = E_i e^{i\omega t}$, and the total reflected field on the same plane is written as $\mathcal{E}_R = E_r e^{i\omega_{dr} t}$, then $\omega$ and $\omega_{dr}$ are related through the relation [12,13]

$$\omega_{dr} = \omega\frac{c-v_i}{c+v_i}, \tag{7}$$

where $v_i$ is positive when the FPI is moving along the same direction as the incident wave. $E_i$ and $E_r$ are complex amplitudes for incident and reflected fields, respectively. When the FPI moves uniformly, there is a steady relation between $E_r$ and $E_i$, which can be derived through the multiple-wave superposition as shown in Fig. 3(a). It is straightforward to verify that such an analysis results in a general relation

$$E_r = \frac{r(1-e^{-i\delta})}{1-r^2e^{-i\delta}}E_i, \tag{8}$$

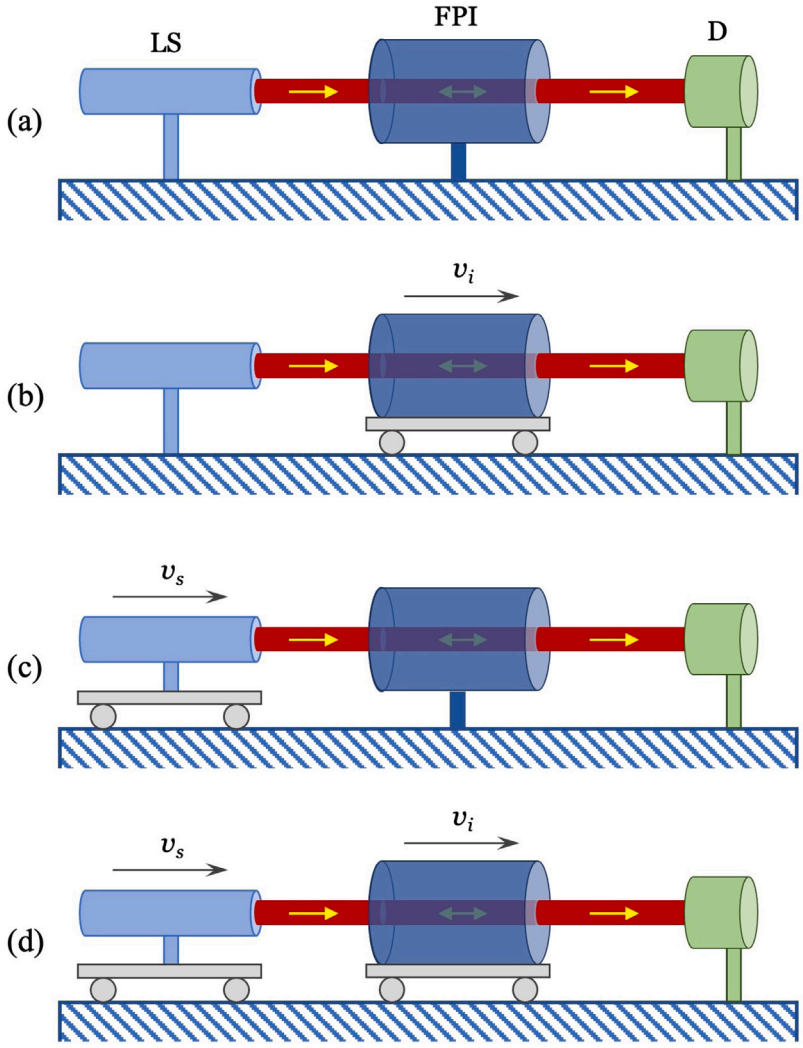


**Fig. 2.** The three key components in the operation system of a passive FPI and the four motion schemes ((a)–(d)) studied in this work. LS: light source, D: detector.

where $\delta$ is the round-trip phase delay in a uniformly moving FPI. To find $\delta$, we follow two consecutive wavefronts $W_1$ and $W_2$ through a round trip, as illustrated in Fig. 3(b). Their phase delay is given by

$$\delta = \frac{\omega_{dr}}{c}(c + v_i)\Delta\tau, \tag{9}$$

where $\Delta\tau$ is the round-trip time of the wavefront $W_2$ inside the FPI. Previously [11], we have shown that $\Delta\tau$ is given by,

$$\Delta\tau = \frac{2nd}{\sqrt{c^2 - v_i^2}}. \tag{10}$$

Applying (7) and (10) to (9) leads to

$$\delta = 2\zeta nkd, \tag{11}$$

which is the same round-trip phase used in the transmission coefficient (5) with $\zeta$ given by (6).

Combining (8) and (11) yields the total reflected field

$$\mathcal{E}_R = \frac{r(1 - e^{-2i\zeta nkd})}{1 - r^2 e^{-2i\zeta nkd}} E_i e^{i\omega_{dr} t}. \tag{12}$$

Taking the ratio of $\mathcal{E}_R$ and $\mathcal{E}_I$ results in the reflection coefficient of a uniformly moving FPI

$$R = \frac{r(1 - e^{-2i\zeta nkd})}{1 - r^2 e^{-2i\zeta nkd}} e^{-2i\left(\frac{v_i}{c}\right)\omega t}, \tag{13}$$

where the nonrelativistic condition $v_i \ll c$ has been used to simplify the Doppler-shift term. This coefficient (13) clearly shows the impact of motion to the reflected field in two aspects: (i) a velocity-dependent scaling factor $\zeta$ in the round-trip phase (same as the transmission scaling factor), and (ii) a Doppler frequency shift proportional to twice the velocity of the FPI, which does not exist in the transmitted field.

### 2.3. Moving light source and stationary FPI

The next case to be considered is the scenario where the FPI is fixed in the lab frame while the light source is uniformly moving along the optical axis as shown in Fig. 2(c). Since the FPI is stationary relative to the detector, from the observer point of view, its behavior is same as in Case A. The moving light source, however, introduces a Doppler shift that has to be factored in when considering the round-trip phase inside the FPI. With this basic understanding, we can utilize the relations (1) and (2) to construct the transmission coefficient and the reflection coefficient of the FPI as

$$T = \frac{(1 - r^2)e^{-ink_d d}}{1 - r^2 e^{-2ink_d d}}, \tag{14}$$

and

$$R = \frac{r(1 - e^{-2ink_d d})}{1 - r^2 e^{-2ink_d d}}, \tag{15}$$

where $k_d$ is the wave number after the Doppler shift. Given the Doppler-shifted wavelength $\lambda_d = \lambda(1 - v_s/c)$, where $\lambda$ is the actual wavelength of the light source and $v_s$ is the velocity of the light source (positive when

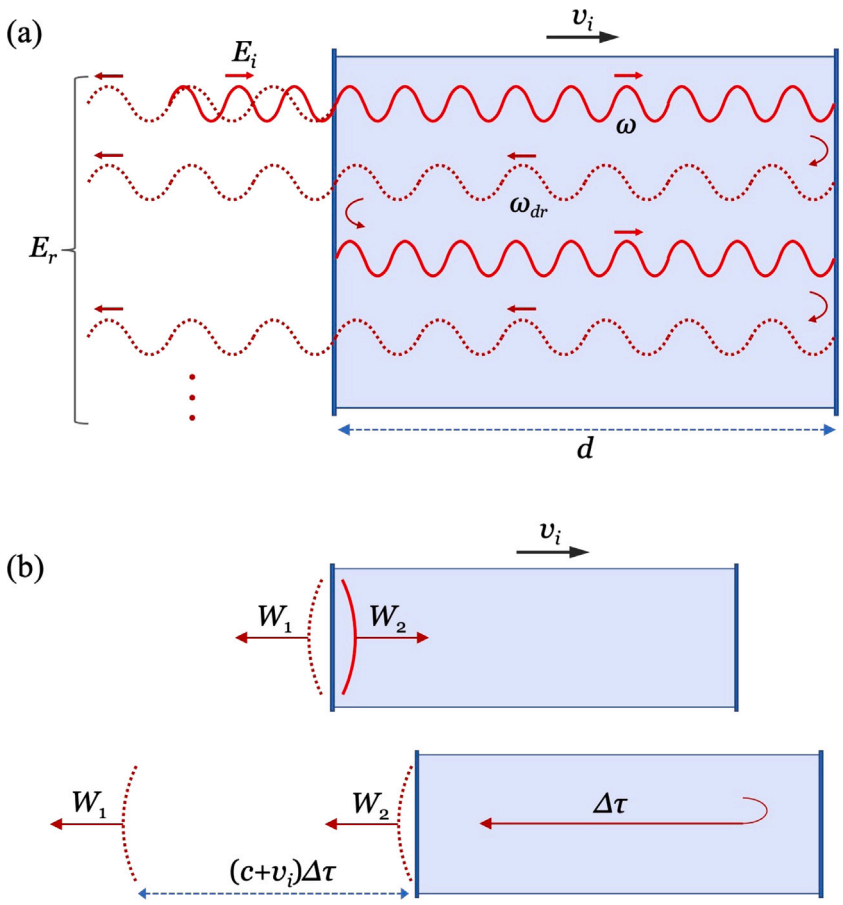


**Fig. 3.** (a) The concept of multiple-wave superposition for a uniformly moving FPI. (b) Finding the round-trip phase delay by following the propagation of a wavefront.

moving toward the FPI), it is straightforward to show that $k_d$ can be written as

$$k_d = k\left(1 + \frac{v_s}{c}\right), \tag{16}$$

where $k = 2\pi/\lambda$ is the wave number when the light source is at rest.

### 2.4. Moving light source and moving FPI

Finally, in the case shown in Fig. 2(d), we analyze the most generic scenario, where both the light source and the FPI move independently along the optical axis in the lab frame, at $v_s$ and $v_i$, respectively. Based on the discussions in the previous sections, we can qualitatively summarize the impacts of motion in the operation of an FPI as: a nonzero velocity of the FPI introduces a scaling factor $\zeta$ in the round-trip phase, while a nonzero velocity of the light source changes the wave number through the Doppler-shifted wavelength.

Since these two processes are independent from each other, it is conceivable that, when they are present at the same time, the overall response of the FPI is a simple combination of the two effects. In the case of transmission, combining (5) and (14) leads to

$$T = \frac{(1-r^2)e^{-i\zeta n k_d d}}{1 - r^2 e^{-2i\zeta n k_d d}}, \tag{17}$$

where $\zeta$ and $k_d$ are defined by (6) and (16), respectively. For reflection, a similar treatment to (13) and (15) yields

$$R = \frac{r(1 - e^{-2i\zeta n k_d d})}{1 - r^2 e^{-2i\zeta n k_d d}} e^{-2i\left(\frac{v_i}{c}\right)\omega t}. \tag{18}$$

In the end, we summarize the latter three cases by giving the general form of the transmittance and the reflectance of the FPI when motion is considered. Comparing (17) and (18) with (1) and (2), it immediately becomes clear that a straightforward generalization of (3) and (4) leads to

$$|T|^2 = \frac{1}{1 + (2\mathcal{F}/\pi)^2 \sin^2(\zeta n k_d d)}, \tag{19}$$

and

$$|R|^2 = \frac{(2\mathcal{F}/\pi)^2 \sin^2(\zeta n k_d d)}{1 + (2\mathcal{F}/\pi)^2 \sin^2(\zeta n k_d d)}. \tag{20}$$

## 3. Impact of motion in PDH frequency locking

To demonstrate the application of this general theory, let us evaluate the impact of motion in a PDH frequency locking system [14]. The PDH technique has been widely used in fields such as laser frequency stabilization [15,16], precision metrology [17,18], and optical sensing [19,20]. Its operation involves comparing the laser frequency with a resonance peak of a reference FPI and subsequently generating an error signal that is proportional to this frequency difference [21]. The error signal is then used to correct the laser frequency through a feedback system. Prior work investigating frequency shifts and excess noise in PDH locking focused primarily on fluctuations in cavity length [22–24]. No work has been reported on the motion of the cavity as a whole.

For the purpose of the current analysis, we neglect the ancillary components of the PDH system such as the electro-optic modulator and all the electronics, keeping only the core optical components: a laser, an FPI, a beamsplitter and a photodetector. A conceptual layout of the scheme is shown in Fig. 4. We further assume that the laser and the FPI can move along their common optical axis while the beamsplitter and the photodetector remain stationary in the lab frame.

Once again, we will start with simpler cases and gradually proceed toward more complex situations.

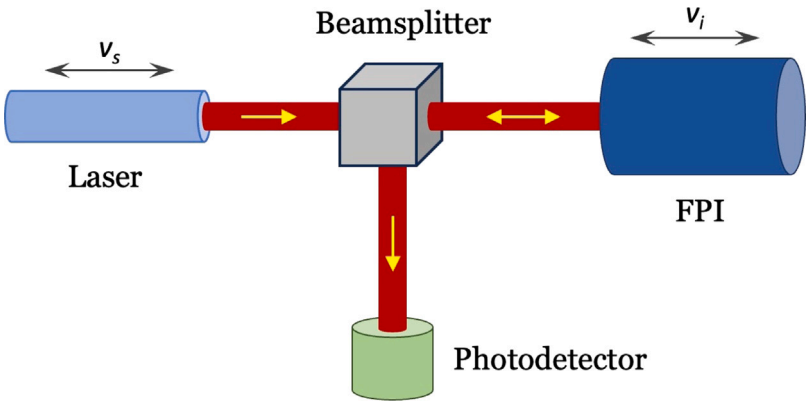


**Fig. 4.** Simplified optical layout for a typical Pound-Drever-Hall frequency locking system. In the current discussion, the laser and the FPI are considered movable in the longitudinal direction.

### 3.1. Only laser moves

Let us first examine the case with a moving laser and a fixed FPI (see Fig. 2(c)). The reflection coefficient of the FPI is given by (15). Following the discussions and notations outlined by Black [21] while incorporating (16), we rewrite the round-trip phase as

$$\delta = 2nk_d d = \frac{\omega + \delta\omega_s}{\Delta\nu_{fsr}}, \tag{21}$$

where $\omega$ is the original frequency of the laser, i.e., the frequency in its rest frame, $\delta\omega_s = \omega(v_s/c)$ is the Doppler shift caused by the laser movement, and $\Delta\nu_{fsr} = c/(2nd)$ is the free spectral range of the FPI. Eq. (21) suggests that a longitudinal motion of the laser effectively introduces a frequency drift to the laser, which is proportional to the velocity of the movement. For a PDH locking system, such a frequency drift is indistinguishable from an intrinsic laser frequency change. In other words, the motion effectively adds a velocity-induced frequency noise to the laser.

### 3.2. Only FPI moves

Next, we analyze the case where the laser is fixed while the FPI is moving (see Fig. 2(b)). This scenario is more complex because two factors are involved in the process: an oscillation term representing a Doppler shift of $-2(v_i/c)\omega$ and a rescaling factor $\zeta$ in the round-trip phase, as pointed out earlier in Section 2. B.

First, let us focus on the reflection-induced Doppler term $\exp[-2i(v_i/c)\omega t]$. It introduces a universal frequency shift to any wave reflected by the FPI. In the PDH scheme, the wave incident in the FPI is a frequency-modulated (FM) optical carrier [14,21]. It has been shown that a periodically modulated wave reflected off a uniformly moving target remains as a periodically modulated wave, but with a Doppler-shifted modulation frequency [25,26]. This feature can be easily seen in the current context by inspecting how the optical carrier and its two FM sidebands change frequencies upon reflection from the FPI. If we denote the frequency of the laser as $\omega$ and the frequencies of the FM sidebands as $\omega + \Omega$ and $\omega - \Omega$, where $\Omega$ is the modulation frequency of the electro-optic modulator, then according to (13), a reflection off the moving FPI causes the three frequencies to shift to

$$\begin{cases} \omega \to \omega + K\omega = (1+K)\omega, \\ \omega + \Omega \to (\omega+\Omega) + K(\omega+\Omega) = (1+K)\omega + (1+K)\Omega, \\ \omega - \Omega \to (\omega-\Omega) + K(\omega-\Omega) = (1+K)\omega - (1+K)\Omega, \end{cases} \tag{22}$$

where $K = -2(v_i/c)$. It is evident from the above result that the light reflected off a moving FPI contains a Doppler-shifted optical carrier $(1+K)\omega$ and a Doppler-shifted FM frequency $(1+K)\Omega$. Since the PDH technique is insensitive to the carrier frequency [21], the impact of the Doppler term $\exp[-2i(v_i/c)\omega t]$ is mainly contributed by the FM frequency shift $K\Omega$. In principle, such a change would introduce additional noise to the PDH error signal through the subsequent homodyne process. Practically, the severity of this additional noise depends on the velocity of the FPI, as well as the noise budget of the locking system. As will be shown later, a reasonable speed range for the FPI is on the order of mm/s or cm/s. This leads to a $K$ factor of the order of $10^{-11} - 10^{-10}$. The absolute frequency shift for a typical FM frequency $\Omega = 10\,\text{MHz}$ is about $0.1 - 1\,\text{mHz}$. For most common applications, this level of uncertainty can be well within the tolerable range.

The second effect caused by a moving FPI is the velocity-dependent scaling factor $\zeta$. It is not hard to see by comparing (13) and (15) that $\zeta$ and $k_d$ play similar roles in the FPI reflection coefficient, namely adding a Doppler drift to the optical frequency. This becomes more clear when (6) is rewritten as $\zeta \approx (1 - v_i/c)$ and substituted into the round-trip phase given by (11), which yields

$$\delta = \frac{\omega - \delta\omega_i}{\Delta\nu_{fsr}}, \tag{23}$$

where $\delta\omega_i = \omega(v_i/c)$ is an equivalent Doppler drift in the optical frequency. Note that this result is consistent with our previous report, in which we concluded that a nonzero velocity of the FPI would rescale its resonance peaks by a factor of $(1 + v_i/c)$ [11].

### 3.3. Both laser and FPI move

Finally, we discuss the general case where both the laser and the FPI are moving (see Fig. 2(d)). A quick comparison of the general reflection coefficient (18) with the previous two cases (13) and (15) indicates that the overall impact of these motions on a PDH locking system combines all the effects considered above. Of particular interest here is the overall round-trip phase, where two separate Doppler drifts must be factored in. Combining (11), (21) and (23), it is straightforward to show that the general round-trip phase is given by

$$\delta = \frac{\omega}{\Delta\nu_{fsr}}\left(1 - \frac{v_i}{c}\right)\left(1 + \frac{v_s}{c}\right) \approx \frac{\omega - \delta\omega_i + \delta\omega_s}{\Delta\nu_{fsr}}, \tag{24}$$

where the second-order term has been neglected. Evidently, the motions of both the laser and the FPI contribute to the overall frequency drift. The different signs between $\delta\omega_i$ and $\delta\omega_s$ are simply due to the different definitions of positive $v_i$ and $v_s$.

An interesting observation is worth being pointed out here. When $v_i$ and $v_s$ are equal and in the same direction, the $\delta\omega_i$ and $\delta\omega_s$ terms in (24) cancel out, leaving $\delta \approx \omega/\Delta\nu_{fsr} = 2nkd$ taking the form as if the laser and the FPI are both stationary. This suggests that, by keeping the laser and the FPI relatively stationary to each other, the impact of velocity can be mitigated. In other words, a relative motion between the detector and the laser-FPI pair is far less influential to the PDH error signal than a relative motion between the detector and either the laser or the FPI individually.

### 3.4. Discussions

In reality, it is highly unlikely that a PDH system involves uniformly moving components. A more realistic scenario has to do with the mechanical vibration of the optical fixtures. Optical components, as well as their mounting and storage structures, are inevitably subject to spontaneous vibrations. The impacts of such vibrations have been extensively studied [7–10], but never from a velocity point of view. Although an in-depth analysis based on first principles is beyond the scope of this report, we can nevertheless utilize the results developed above to loosely gauge the scales of the excess noises caused by vibration velocities.

Suppose that one of the optical components (laser or FPI) is mounted on a mechanical structure that vibrates in the direction of the laser beam at an intrinsic resonance frequency of 1 kHz, with a peak-to-peak amplitude of 1 μm. Vibrations of such a scale are quite common in optical structures [27,28]. According to (24), a frequency modulation at 1 kHz is effectively added to the laser frequency. To evaluate the scale of this additional frequency noise, we use the peak-to-peak velocity swing $\Delta v_{pp}$ as an indicator, and $\Delta v_{pp} \sim 6$ mm/s in the current case, which leads to a Doppler ratio $\Delta v_{pp}/c \sim 2 \times 10^{-11}$. For a typical laser frequency at 400 THz (750 nm), the corresponding frequency swing is about 8 kHz. This level of excess FM noise is non-negligible for today's narrow-linewidth lasers, which are often employed in high-precision PDH locking systems [29]. An important consequence of this additional noise is an increased noise budget for the locking electronics. In other words, the feedback control system must be equipped with a sufficient bandwidth in order to suppress the velocity-induced frequency fluctuations.

Another way to gauge the impact of Doppler frequency instability is to compare it with an existing frequency instability standard. To do that, we use a commercial FPI frequency reference as an example. Thorlabs/MenloSystems XM-ORC15 is an ultra-stable optical reference cavity that operates at 1064 nm. It is made of an ultra-low expansion (ULE) glass body of 12.1 cm and has a specified thermal noise Allan deviation limit (ADEV) of $1.6 \times 10^{-16}$ when averaged over 1 s [30]. If the cavity mounting structure experiences vibrations, motion-induced fluctuations will be added to the overall frequency instability. To assess the impact of the vibration, we can calculate how much vibration can cause a fractional frequency uncertainty that rivals the thermal noise ADEV. Following the same strategy as in the above example, it is easy to show that the peak-to-peak fractional frequency fluctuation induced by a harmonic vibration is given by $2\pi\Delta x_{pp} f/c$, where $\Delta x_{pp}$ is the peak-to-peak vibration amplitude and $f$ is the vibration frequency. We are particularly interested in vibration at $f = 0.5$ Hz here because it can create the greatest frame-to-frame frequency swing when frequencies are measured with a 1-s averaging time. To keep this vibration-induced frequency uncertainty below the thermal noise limit ($1.6 \times 10^{-16}$), the estimated vibration amplitude is $\Delta x_{pp} \approx 0.02$ μm. In reality, such small mechanical vibrations could be difficult to completely prevent.

Finally, it is worth stressing again that the above evaluation is based on the assumption of a rigid FPI without deformation. The only displacements considered here are those caused by the relative movements between different optical components. Under conventional theory, such displacements would not directly impact the frequency accuracy of a PDH system because neither the laser nor the FPI incurs any frequency change. Therefore, by factoring in the effects of velocity, this generalized FPI theory reveals a new aspect of the PDH scheme that can be nontrivial in certain applications.

## 4. Conclusion

In conclusion, we have formulated an expanded theory to describe the transmission and reflection behaviors of an FPI when key optical components in its operating system move relative to each other along their common optical axis. Our analysis shows that, when the light source and the FPI move independently against the detector (observer), they each introduce a velocity-dependent factor in the FPI round-trip phase, which effectively adds a Doppler shift to the transmission and the reflection coefficients. An independent FPI motion, meanwhile, exerts an additional global frequency shift proportional to $-2(v_i/c)$ on the reflected wave. On the other hand, when the light source and the FPI move together against the detector, their effects on the round-trip phase cancel out, leading to a much reduced velocity sensitivity. To showcase the applications of this generalized theory, we have investigated the potential impact of velocity-induced excess noise in PDH laser frequency locking. Our evaluation indicates that tiny mechanical vibrations of the laser and the FPI can effectively introduce additional FM noise to the laser frequency, which should be taken into account in high-precision laser frequency stabilization. Overall, it is our hope that this work helps bring necessary attention to the overlooked aspect of velocity-induced effects in metrological systems involving the FPI.

## CRediT authorship contribution statement

**Lingze Duan:** Writing – review & editing, Writing – original draft, Validation, Resources, Project administration, Methodology, Investigation, Formal analysis, Conceptualization.

## Declaration of competing interest

The authors declare that they have no known competing financial interests or personal relationships that could have appeared to influence the work reported in this paper.

## Data availability

No data was used for the research described in the article.

## References

[1] J.M. Vaughan, The Fabry-Perot Inteferometer: History, Theory, Practice and Applications, first ed., Routledge, 1989, http://dx.doi.org/10.1201/9780203736715.
[2] C. Fabry, A. Perot, Theorie et applications d'une nouvelle methode de Spectroscopie Interferentielle, Ann. Chim. Phys. 16 (1899) 115.
[3] B.P. Abbott, LIGO: the laser interferometer gravitational-wave observatory, Rep. Progr. Phys. 72 (7) (2009) 076901, http://dx.doi.org/10.1088/0034-4885/72/7/076901.
[4] C. Gräf, S. Hild, H. Lück, B. Willke, K.A. Strain, S. Goßler, K. Danzmann, Optical layout for a 10 m Fabry-Pérot Michelson interferometer with tunable stability, Classical Quantum Gravity 29 (7) (2012) 075003, http://dx.doi.org/10.1088/0264-9381/29/7/075003.
[5] T.A. Al-Saeed, D.A. Khalil, Characteristics of a refractometer based on Michelson interferometer integrated with a Fabry-Perot interferometer, Optik 242 (1) (2021) 167170, http://dx.doi.org/10.1016/j.ijleo.2021.167170.
[6] N.M.R. Hoque, L. Duan, A Mach-Zehnder Fabry-Perot hybrid fiber-optic interferometer operating at the thermal noise limit, Sci. Rep. 12 (1) (2022) 12130, http://dx.doi.org/10.1038/s41598-022-16474-y.
[7] Y.Y. Jiang, A.D. Ludlow, N.D. Lemke, R.W. Fox, J.A. Sherman, L.S. Ma, C.W. Oates, Making optical atomic clocks more stable with 10 -16-level laser stabilization, Nat. Photonics 5 (3) (2011) 158–161.
[8] L. Chen, J.L. Hall, J. Ye, T. Yang, E. Zang, T. Li, Vibration-induced elastic deformation of Fabry-Perot cavities, Phys. Rev. A 74 (5) (2006) 053801.
[9] I. Jeon, C. Ahn, C. Kim, S. Park, W. Jeon, L. Duan, J. Kim, Palm-sized, vibration-insensitive, and vacuum-free all-fiber-photonic module for 10 -14-level stabilization of CW lasers and frequency combs, APL Photonics 8 (12) (2023) 120804.
[10] C.T. Taylor, M. Notcutt, D.G. Blair, Cryogenic, all-sapphire, Fabry–Perot optical frequency reference, Rev. Sci. Instrum. 66 (2) (1995) 955–960.
[11] N. Pyvovar, L. Duan, Optical transmission of a moving Fabry–Perot interferometer, Opt. Lett. 49 (2) (2024) 359–362, http://dx.doi.org/10.1364/OL.505622.
[12] H.E. Ives, The Doppler effect from moving mirrors, J. Opt. Soc. Am. 30 (6) (1940) 255–257.
[13] B.M. Bolotovskiĭ, S.N. Stolyarov, Reflection of light from a moving mirror and related problems, Sov. Phys. Uspekhi 32 (9) (1989) 813–827.

[14] R.W. Drever, J.L. Hall, F.V. Kowalski, J. Hough, G.M. Ford, A.J. Munley, H. Ward, Laser phase and frequency stabilization using an optical resonator, Appl. Phys. B 31 (1983) 97–105.
[15] C. Salomon, D. Hils, J.L. Hall, Laser stabilization at the millihertz level, J. Opt. Soc. Am. B 5 (8) (1988) 1576–1587.
[16] L. Duan, K. Gibble, Locking lasers with large FM noise to high-Q cavities, Opt. Lett. 30 (24) (2005) 3317–3319, http://dx.doi.org/10.1364/OL.30.003317.
[17] P.W. McNamara, Weak-light phase locking for LISA, Classical Quantum Gravity 22 (10) (2005) S243.
[18] J.R. Lawall, Fabry–Perot metrology for displacements up to 50 mm, J. Opt. Soc. Amer. A 22 (12) (2005) 2786–2798.
[19] X. Zhan, Z. Wang, S. Kumar, C. Marques, X. Li, R. Min, The application of Pound–Drever–Hall technology in high-resolution sensing—A review, IEEE Sens. J. 23 (7) (2023) 6427–6438.
[20] N.M.R. Hoque, L. Duan, Ultrahigh-resolution fiber-optic sensing based on high-finesse, meter-long fiber Fabry-Perot resonators, IEEE Photonics J. 12 (3) (2020) 1–9.
[21] E.D. Black, An introduction to Pound–Drever–Hall laser frequency stabilization, Am. J. Phys. 69 (1) (2001) 79–87, http://dx.doi.org/10.1119/1.1286663.
[22] S. Schiller, S.U. Seel, R. Storz, J. Mlynek, Experimental studies of cryogenic optical resonators, in: Laser Frequency Stabilization and Noise Reduction, Vol. SPIE 2378, 1995, pp. 138–146.
[23] Y. Levin, Internal thermal noise in the LIGO test masses: A direct approach, Phys. Rev. D 57 (2) (1998) 659–663.
[24] T. Kessler, T. Legero, U. Sterr, Thermal noise in optical cavities revisited, J. Opt. Soc. Am. B 29 (1) (2012) 178–184.
[25] V.S. Sobolev, E.N. Utkin, G.A. Kashcheeva, F.A. Zhuravel, A.M. Shcherbachenko, Doppler shift of the modulation frequency of laser radiation scattered by a moving object, Opt. Spectrosc. 119 (2) (2015) 291–294.
[26] K. Sung, M. Majji, Doppler measurement of modulated light for high speed vehicles, Sensors 22 (4) (2022) 1444.
[27] R.L. Forward, Electronic damping of vibrations in optical structures, Appl. Opt. 18 (5) (1979) 690–697.
[28] P. Nachman, P.M. Pellegrino, A.C. Bernstein, Mechanical resonance detected with a Michelson interferometer, Am. J. Phys. 65 (5) (1997) 441–443.
[29] W. Zhang, L. Stern, D. Carlson, D. Bopp, Z. Newman, S. Kang, J. Kitching, S.B. Papp, Ultranarrow linewidth photonic-atomic laser, Laser Photonics Rev. 14 (4) (2020) 1900293.
[30] Thorlabs, Optical reference cavities with crystalline mirrors, 2025, URL https://www.menlosystems.com/products/ultrastable-lasers/xm-orc/.